J. Fluid Mech. (2010), *vol.* 654, *pp.* 363–386.
doi:10.1017/S0022112010000637

Experimental and numerical study of the wave run-up along a vertical plate

B. MOLIN[1]†, O. KIMMOUN[1], Y. LIU[1], F. REMY[1] AND H. B. BINGHAM[2]

[1]École Centrale Marseille and Institut de Recherche sur les Phénomènes Hors Equilibre (IRPHE), 13451 Marseille cedex 20, France

[2]Department of Mechanical Engineering, Technical University of Denmark, DK-2800 Kongens Lyngby, Denmark

(Received 16 September 2009; revised 25 January 2010; accepted 1 February 2010; first published online 13 May 2010)

Results from experiments on wave interaction with a rigid vertical plate are reported. The 5 m long plate is set against the wall of a 30 m wide basin, at 100 m from the wavemaker. This set-up is equivalent to a 10 m plate in the middle of a 60 m wide basin. Regular waves are produced, with wavelengths of 1.6 m, 1.8 m and 2 m, and steepnesses H/L (H being the double amplitude and L being the wavelength) ranging from 2 % to 5 %. Free-surface elevations along the plate are measured with a row of 20 gauges. The focus is on the time evolution of the free-surface profile along the plate. At all steepnesses, strong deviations from the predictions of linear theory gradually take place as the reflected wave field develops in the basin. This phenomenon is attributed to third-order interactions between the incoming and reflected wave systems, on the weather side of the plate. The measured profiles along the plate are compared with the predictions of two numerical models: an approximate model based on the tertiary interaction theory of Longuet-Higgins & Phillips (*J. Fluid Mech.*, vol. 12, 1962, p. 333) for plane waves, which provides a steady-state solution, and a fully nonlinear numerical wavetank based on extended Boussinesq equations. In most of the experimental tests, despite the large distance from the wavemaker to the plate and the small amplitude of the incident wave, no steady state is attained by the end of the exploitable part of the records.

1. Introduction

Our recent work has been concerned with wave interaction with strongly reflective structures. This has followed a series of experiments, in the same facility (CEHIPAR) as for the tests presented here, on the roll response of barges in beam seas: very high free-surface elevations could be observed at mid hull of the barge model, in complete disagreement with the predictions of linear theory. Recently, similar observations (with an oil tanker model) have been reported by Spentza & Swan (2009), in an experimental investigation related to the Prestige disaster.

Following the barge model tests, we carried out several experimental campaigns with simpler models in the shape of rigidly held vertical plates. First results are reported in Molin *et al.* (2005*b*): a 1.2 m long plate was set against the wall of a

† Email address for correspondence: bernard.molin@ec-marseille.fr

16 m wide tank (Bassin de Génie Océanique (BGO)- First in la Seyne-sur-mer), at a distance of about 20 m from the wavemaker. This set-up was equivalent to a 2.4 m plate in the middle of a 32 m wide basin. The plate was subjected to regular waves of varying periods and amplitudes, with wavelengths L ranging from 1 m to 3 m, and wave steepnesses H/L ranging from 2 % to 6 %. Very high wave elevations were observed on the plate by the wall corner, with response amplitude operators (RAOs) taking values up to 5, which is more than twice the values predicted by linearized potential flow theory.

It was advocated that these phenomena are due to tertiary (third-order) interactions between the incoming and reflected wave systems: the reflected waves 'slow down' the incoming waves, acting in the same way as a shoal, inducing energy focusing effects. On the basis of the theoretical analysis of Longuet-Higgins & Phillips (1962) for plane waves, an approximate numerical model was proposed: the space evolution of the complex amplitude of the incoming waves, as they progress towards the plate and interact with the reflected wave system, is described by a simple parabolic equation. This equation is solved starting some distance ahead of the plate (e.g. the wavemaker line), and over some width (e.g. the basin width). Incoming and reflected wave systems are successively updated through an iterative process, until convergence is reached. Good agreement was found between measured and calculated free-surface profiles along the plate.

Molin *et al.* (2006) report another series of experiments, in the same facility, with a longer plate (3 m) and shorter wavelengths (0.6–2 m). Experimental RAOs of the free-surface elevation along the plate are compared with numerical results from the parabolic model of Molin *et al.* (2005*b*), and from a fully nonlinear numerical wavetank based on extended Boussinesq equations (Jamois *et al.* 2006). The Boussinesq model closely reproduces the time evolution of the free-surface profile along the plate. A short-coming of the experiments is that the exploitable time window is limited, due to multiple reflections between the wavemaker and the plate. This duration can be too short for a steady state to be reached. Another concern is that the 20 m distance from the wavemaker to the plate may be too short for the nonlinear interactions between the incoming and reflected waves to have fully evolved. As a matter of fact, numerical runs with the parabolic model suggest that the effective interaction area can be very large, especially in the case of small wavelengths and small steepnesses. When the steepness increases and/or the wavelength over plate length ratio decreases, the iterative scheme fails to converge, raising the question of whether or not a steady state can ever be reached. When the iterative scheme does converge, it may also be wondered whether the obtained solution is unique.

These questions motivated the present study, which consisted of another experimental campaign carried out in the Ship Dynamics Laboratory of CEHIPAR in Spain. The tank size is 150×30 m. The set-up was similar to the previous ones, a vertical plate, 5 m long, protruding from the wall at a large distance from the wavemaker. Tests were carried out in regular and irregular waves. In this paper we report the regular wave tests only. In § 2, we briefly describe the two numerical models, based on the parabolic approximation and the extended Boussinesq equations. More detailed information may be found in Jamois *et al.* (2006) and Molin *et al.* (2005*b*). In § 3, the experimental campaign is described and some typical results are presented. In § 4, we first analyse the tests at the 1.01 s wave period. The time evolutions of the free-surface RAOs, at the different gauges along the plate, are shown and compared with the predictions of the parabolic model. The Boussinesq model is run for three cases of the 1.13 s wave period tests, at the lowest wave steepnesses.

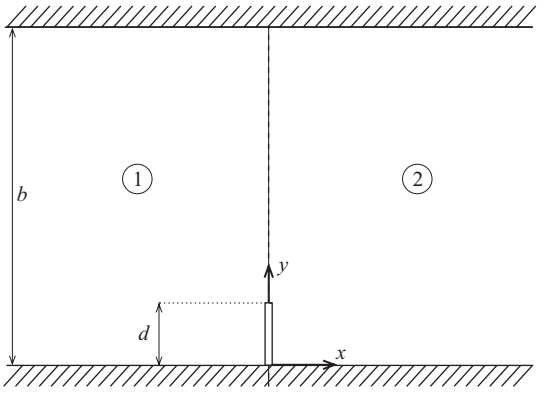

FIGURE 1. Geometry.

2. The numerical models

2.1. *The parabolic model*

We refer to Molin *et al.* (2005*b*) for a detailed description. The resolution is done in the frequency domain with the velocity potential expressed as

$$\phi(x, y, z, t) = \mathrm{Re}\left\{\varphi(x, y, z)\,\mathrm{e}^{-\mathrm{i}\omega t}\right\}, \tag{2.1}$$

and harmonics at frequencies $n\,\omega$ being discarded.

Here we use a right-handed coordinate system $Oxyz$ with $z=0$ as the free surface at rest, $x=0$, $y=0$ as the intersection between the wall and the plate (figure 1).

The velocity potential φ is decomposed into an incoming component φ_I and a reflected component φ_D. The incoming component is assumed to be in the form

$$\varphi_I = \frac{-\mathrm{i}\,A(\varepsilon^2 x, \varepsilon y)\,g}{\omega}\,\mathrm{e}^{\mathrm{i}k(1-\varepsilon^2)x}\,\mathrm{e}^{\left[k+\varepsilon^2 k_1^{(2)}(\varepsilon^2 x, \varepsilon y)\right]z} \tag{2.2}$$

with ε as the wave steepness expressed as $k\,A_I$, k as the wavenumber ω^2/g and A_I as the incoming wave amplitude at infinity. For simplicity, the water depth is assumed here to be infinite; derivations are straightforward in the finite depth case. In (2.2), the wave amplitude A is a complex quantity, slowly varying in space due to tertiary interactions with the reflected wave system from the plate. This reflected wave system is locally associated with a plane wave of (real) amplitude A_R and direction β_R. It can then be shown (Molin *et al.* 2005*b*) that the complex amplitude A obeys the parabolic equation

$$2\,\mathrm{i}k\,A_x + A_{yy} + 2k^4\left[A_R^2\,f(\beta_R) + A_I^2 - \|A\|^2\right]A = 0 \tag{2.3}$$

where, in infinite water depth (Longuet-Higgins & Phillips 1962),

$$f(\beta) = -\Bigg\{(1-\cos\beta)\sqrt{2+2\cos\beta} + 2\cos\beta + \frac{1}{2}\sin^2\beta + \frac{2(1-\cos\beta)}{\sqrt{2+2\cos\beta}-4}\left(1+\cos\beta+\sqrt{2+2\cos\beta}\right)\Bigg\}. \tag{2.4}$$

Equation (2.3) is similar with the parabolic approximation to the mild slope equation (e.g. see Radder 1979; Dingemans 1997), with the difference that the forcing term is not due to shoaling but to the tertiary interaction with the reflected wave field.

To solve for the diffraction problem and obtain the locally equivalent amplitudes A_R and directions β_R, advantage is taken of the geometry: the fluid domain is decomposed into two semi-infinite domains, on either side of the plate, bounded by the walls of the basin at $y=0$ and $y=b$ (figure 1); in either sub-domain, eigenfunction expansions are used to express the diffraction potential φ_{Di} $(i=1, 2)$ as

$$\varphi_{Di} = \frac{-\mathrm{i}\,Ag}{\omega}\,\mathrm{e}^{kz}\sum_{n=0}^{\infty} B_{in}\,\mathrm{e}^{\pm \mathrm{i}\alpha_n x}\,\cos\lambda_n y, \qquad \lambda_n = n\pi/b, \qquad \alpha_n^2 = k^2 - \lambda_n^2. \quad (2.5)$$

The no-flow condition at the plate ($x=0,\ 0\leqslant y\leqslant d,\ -\infty < z\leqslant 0$) and matching conditions for φ_{D1} and φ_{D2} on the common strip $d<y\leqslant b$ yield the coefficients B_{in}, from which A_R and β_R can be evaluated locally.

We first solve the diffraction problem with the incoming waves unmodified ($A\equiv A_I$). Then the parabolic equation (2.3) is solved numerically starting from some distance l (the 'interaction length') ahead of the plate. This provides an updated incoming wave system at the plate from which a new diffraction problem, and then the parabolic equation, are solved again. This procedure is repeated until some level of convergence is reached. Note that the method used here is quite approximate, first due to the local plane-wave idealization and second due to the fact that modifications of the reflected waves, under their tertiary interaction with the incoming waves, are not accounted for. However, good agreement with the experimental measurements was reported by Molin *et al.* (2005*b*) and Molin *et al.* (2006).

2.2. *The numerical wavetank*

Details are given by Jamois (2005) or Jamois *et al.* (2006). We use the nonlinear free-surface equations in Zakharov form (Zakharov 1968):

$$\eta_t = -\nabla\eta\cdot\nabla\widetilde{\phi} + \widetilde{w}(1+\nabla\eta\cdot\nabla\eta), \quad (2.6)$$

$$\widetilde{\phi}_t = -g\eta - \tfrac{1}{2}(\nabla\widetilde{\phi}\cdot\nabla\widetilde{\phi}) + \tfrac{1}{2}\widetilde{w}^2(1+\nabla\eta\cdot\nabla\eta) \quad (2.7)$$

with $\eta(x, y, t)$ as the free-surface elevation and $\widetilde{\phi}(x, y, t)\equiv\phi(x, y, \eta(x, y, t), t)$ as the velocity potential at the free surface. Similarly, $\widetilde{w}$ is the vertical fluid velocity at the free surface, while ∇ is the horizontal gradient $(\partial/\partial x, \partial/\partial y)$.

To advance η and $\widetilde{\phi}$ in time, the vertical velocity $\widetilde{w}$ is required. This is obtained by expressing the velocity potential ϕ and vertical velocity w as polynomials in z:

$$\phi(x, y, z, t) \approx (1-\alpha_2\nabla^2)\hat{\phi}^* + ((z-\hat{z}) - \beta_3\nabla^2)\hat{w}^*, \quad (2.8)$$

$$w(x, y, z, t) \approx (1-\alpha_2\nabla^2)\hat{w}^* - ((z-\hat{z})\nabla^2 - \beta_3\nabla^4)\hat{\phi}^*, \quad (2.9)$$

with

$$\alpha_2 \equiv \tfrac{1}{2}(z-\hat{z})^2 - \tfrac{1}{10}\hat{z}^2, \qquad \beta_3 \equiv \tfrac{1}{6}(z-\hat{z})^3 - \tfrac{1}{10}\hat{z}^2(z-\hat{z}). \quad (2.10)$$

Equations (2.8) and (2.9) are Padé-enhanced Taylor expansions from a reference level $\hat{z}$, usually taken at mid-depth $-h/2$. The boundary condition at the bottom and (2.8) at the free surface yield a linear system in $(\hat{\phi}^*, \hat{w}^*)$ whose resolution provides w and permits to advance in time. This system of equations allows us to propagate waves over slowly varying bathymetries, while properly accounting for nonlinearity and dispersion up to a non-dimensional water depth kh equal to 10 (Jamois *et al.* 2006). This is the constant depth form of the lowest-order model derived by Bingham, Madsen & Fuhrman (2009), which is based on earlier velocity formulations (e.g. Fuhrman & Bingham 2004).

The incoming regular waves are gradually input, over a wavelength, at the fore end of the numerical domain from a streamfunction solution (Fenton 1988). Reflected

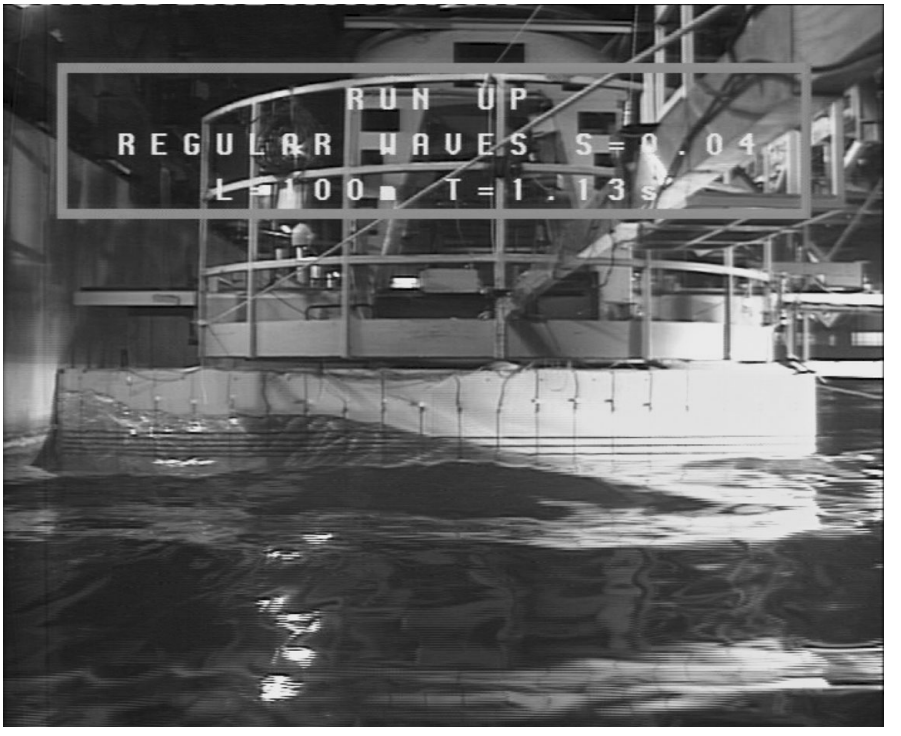

FIGURE 2. The plate in the basin, during tests in regular waves of 1.13 s period and 4 % steepness (note the high free-surface elevation in the wall–plate corner).

waves from the plate are absorbed at the far and fore ends, while they reflect on the lateral wall, as in the physical tank. More details, like the technique used to ensure the no-flow condition on the plate, can be found in the quoted references.

3. The experimental campaign

The experiments took place in the Ship Dynamics Laboratory of CEHIPAR (Canal de Experiencias HIdrodinamicas del PARdo), as part of the HYDRALAB III network project. The tank size is $150 \times 30 \times 5$ m. It is equipped with a segmented wavemaker and a computerized planar motion carriage. The plate model was of size 5×2.33 m, of which 2 m were submerged. It was made of wood, with steel and fiberglass stiffening to prevent any deformation. Twenty resistive wave gauges were set along the plate, every 25 cm with the first one 12.5 cm from the edge (see figure 2). Another gauge was installed 4.87 m away from the plate, at the same distance from the wavemaker, and a last gauge at the lee side of the plate, 2.53 m from the wall and 31.5 cm from the plate.

The specified wave cases included regular and long-crested irregular waves. In this paper, we only consider the regular wave cases. Results from the tests in irregular waves will be reported in a subsequent paper.

Waves were calibrated prior to installing the plate, with gauges every 25 m from the wavemaker all the way to the beach. This allowed us to check the occurrence of Benjamin-Feir instability and to select the plate position accordingly. In the tests reported below at 1.01 and 1.13 s wave periods, the plate was located 100 m away from the wavemaker except for the larger steepness cases. The specified wave periods were 1.01 s, 1.07 s and 1.13 s, that is, according to linear theory, wavelengths of 1.6 m, 1.8 m and 2 m. The specified steepnesses H/L ranged from 2 % up to 5 %, with a 0.5 % spacing.

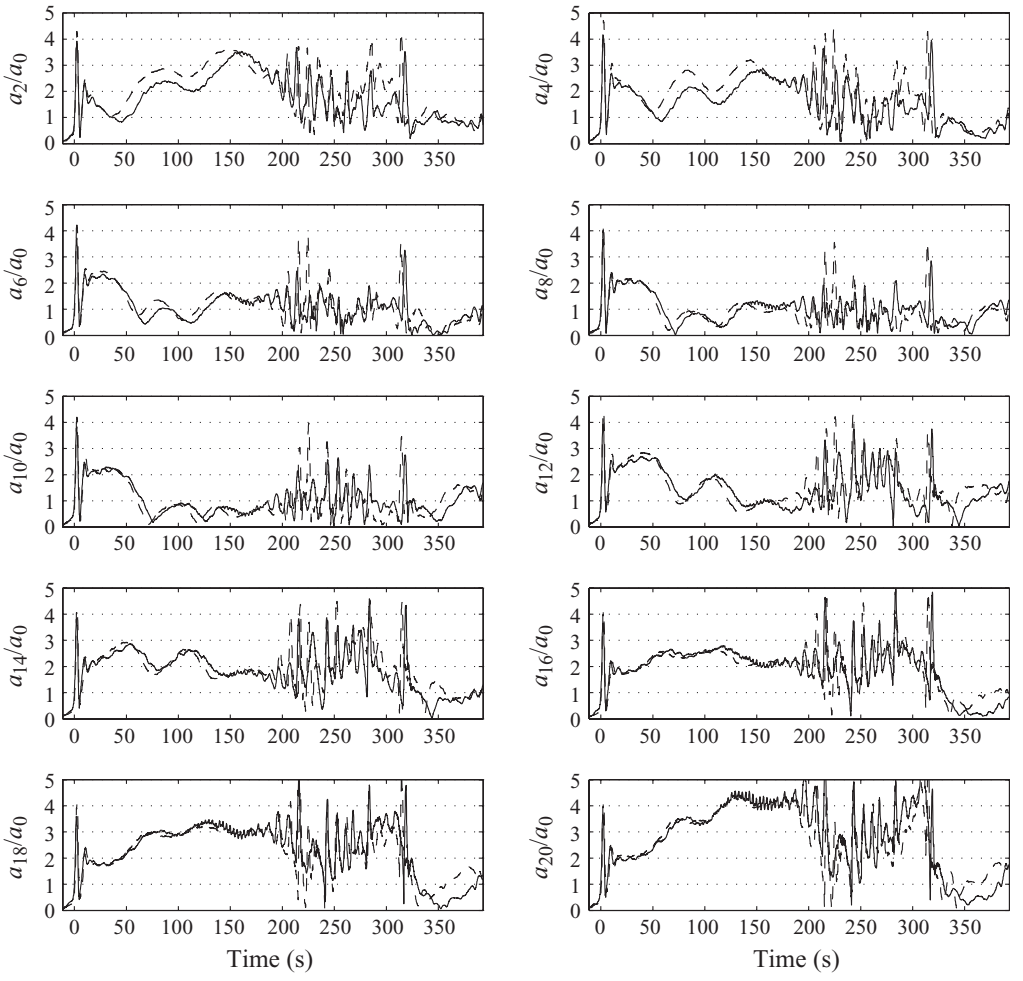

FIGURE 3. Wave period 1.13 s. Steepness $H/L = 3.5\,\%$. Time evolutions of the measured free-surface elevations RAOs at every other gauge from arrival of the wavefront (duplicated test).

Time series of the free-surface elevations as measured at the wave gauges were processed by Fourier analysis over sliding windows, three wave periods long. In this way, time evolutions of the RAOs are obtained.

As an illustration, we consider the case with a wave period of 1.13 s, a steepness H/L of 3.5 %, and the plate at 100 m from the wavemaker. This test was run twice. Figure 3 shows the time evolutions of the RAOs of the free-surface elevations at every other gauge along the plate, from near the edge (gauge 2) to the wall (gauge 20). The wavemaker was activated for about 330 s. On the plots, $t = 0$ corresponds roughly to the arrival of the wavefront. Because the waves travel a long distance, even though their steepness is rather low, the wavefront becomes very steep and modulated, hence the peaks that appear in the plots at $t \sim 0$ s. Similar peaks can be seen after $t \sim 200$ s, they are due to multiple reflections between the plate, wavemaker and sidewalls. According to linear theory, the group velocity is $0.88\,\mathrm{m\,s^{-1}}$, meaning a time window of about 220 s (the distance to the wavemaker was actually 97 m, not 100 m) before re-reflected waves come into play. The plots indicate that disturbances

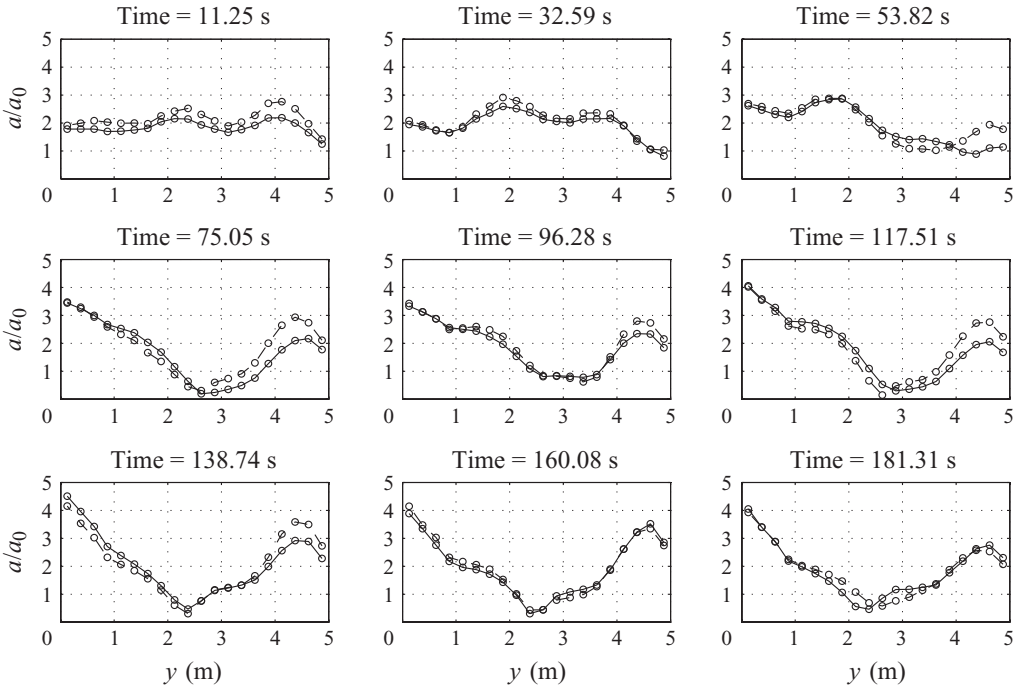

FIGURE 4. Wave period 1.13 s. Steepness $H/L = 3.5\,\%$. Free-surface RAOs along the plate at different instants.

occur somewhat earlier. The importance of reflections can also be seen from the plots at $t > 330$ s: even though the wavemaker was turned off more than 100 s earlier, a strong free-surface motion persists for a long time. Thus, the exploitable part of the time series is only the first 200–220 s.

Considering that part of the plots in figure 3, it can first be observed that the time evolutions of the RAOs, as derived from the two tests, are not identical. Presumably this is due to the basin not being perfectly quiet at the beginning of the tests: although more than 30 min were spent between consecutive tests, there always remained some disturbances in the basin. Another feature is that the time evolutions are not monotonic: the plots exhibit oscillations. It does not appear that a steady state has been attained by the end of the 200 s time window. Only the last gauges by the wall have apparently reached some kind of plateau. Very high values of the RAOs are attained there, up to 4. High free-surface elevations are also observed by the plate edge, while in between very low RAO values are obtained.

Figure 4 shows the same results in a different way, that is the RAOs along the plate at different instants, just after the arrival of the wavefront until just before re-reflections come into play. Over the last three instants ($t = 138.74$, 160.08, 181.31 s), the shapes vary little, and the two tests are in fair agreement. The time evolution of the wave envelope profile, along the plate, is striking. As will be shown later, it is only over the first instants ($t = 11.25$ s in figure 4) that it agrees with the predictions of linear theory. Quite noticeable is the trough that gradually appears at about mid-distance from the edge ($y = 5$ m) to the wall ($y = 0$ m), and the high RAO values that are finally obtained at the wall, around 4, that is about twice the value predicted by the linear theory.

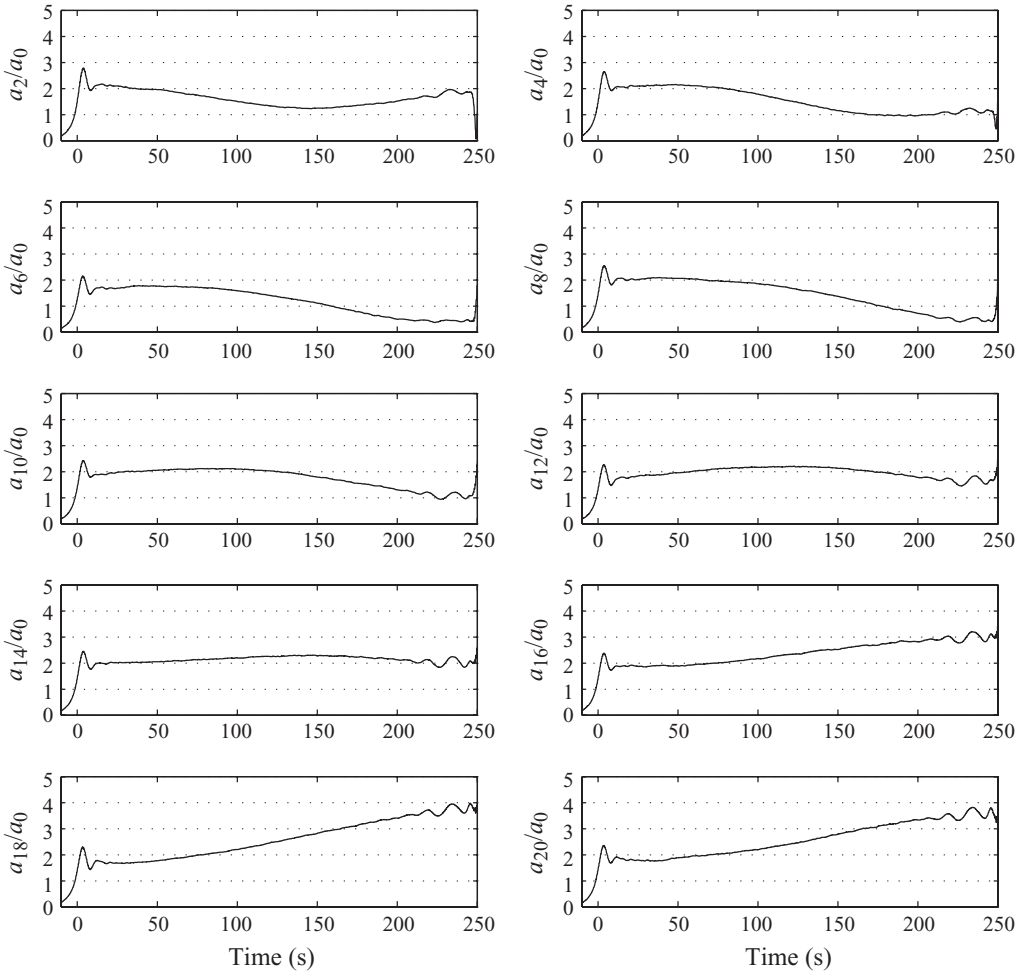

FIGURE 5. Wave period 1.01 s. Steepness $H/L = 2\,\%$. Time evolutions of the measured free-surface elevations RAOs at every other gauge from arrival of the wavefront.

4. Analysis of the results from the experiments and comparisons with computations

We will concentrate on the tests performed at the two wave periods of 1.01 s and 1.13 s, with the plate located at 100 m from the wavemaker. The associated wavelengths, according to linear theory, are 1.6 m and 2 m. This means, respectively, 6.25 and 5 wavelengths along the plate plus mirror plate, and distances of 62.5 and 50 wavelengths from the wavemaker to the plate. The Boussinesq model was run only in the 1.13 s case, which is already quite demanding on computer resources. The parabolic model was run at both wave periods.

4.1. *Regular wave tests at* 1.01 *s period*

At this wave period, the group velocity, according to linear theory, is $0.79\,\mathrm{m\,s^{-1}}$, that is a time window of about 250 s before re-reflections come into play.

Figure 5 shows the time evolution of the RAOs of the free-surface elevations at every other gauge along the plate, at the 2 % wave steepness. The evolution is rather slow but the RAO values have changed dramatically after 200 s. From then on, due to

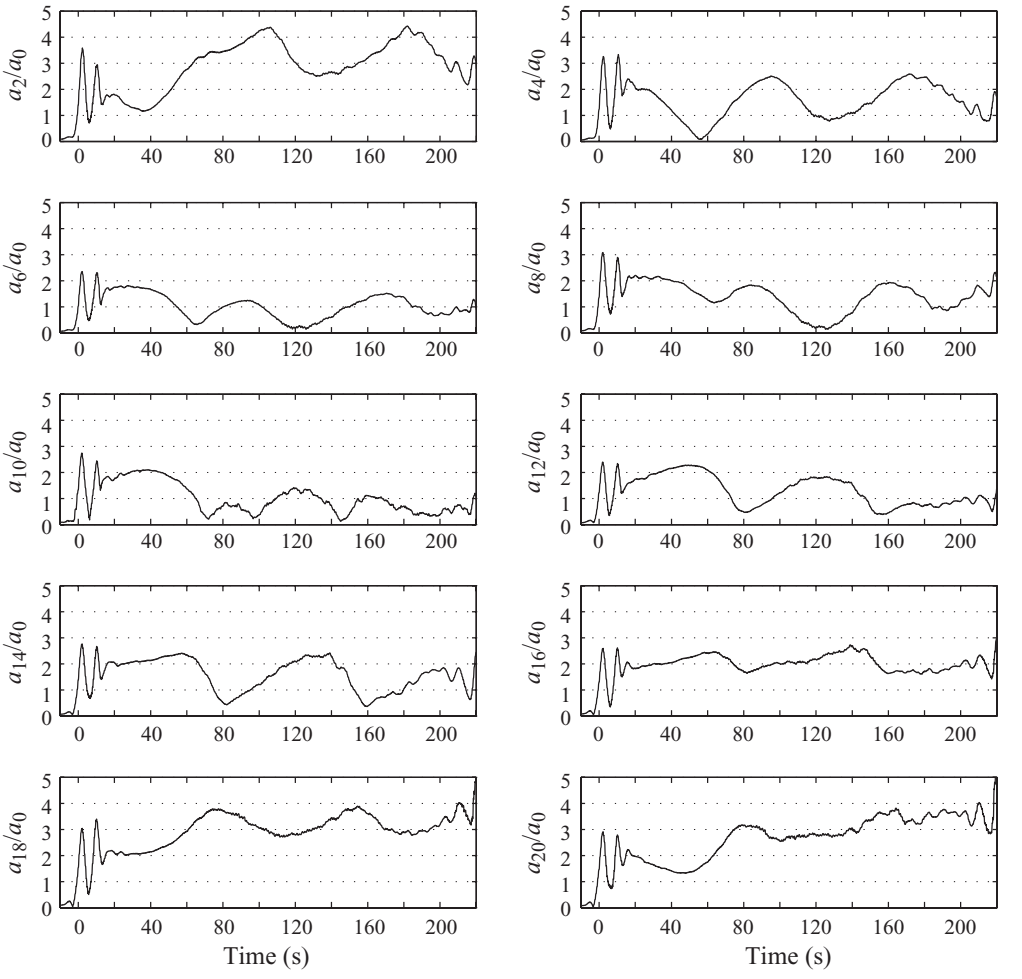

FIGURE 6. Wave period 1.01 s. Steepness $H/L = 3.5\,\%$. Time evolutions of measured the free-surface elevations RAOs at every other gauge from arrival of the wavefront.

the re-reflections, some oscillations start appearing. From the plots, it is not obvious that a steady state has been reached at this stage.

Figure 6 shows the same signals for the 3.5 % wave steepness. As compared with the previous case, the time evolution is faster and quite oscillatory. Re-reflections come into play a little bit earlier (the group velocity increases with the steepness). Obviously, no steady state has been reached after 200 s, and it does not look like the oscillations are finally going to damp out. Note the strong similarity of these plots with those shown in figure 3, at the same wave steepness of 3.5 % but at a different wave period: the observed phenomena are not that sensitive to the precise value of the wavelength as compared to the plate or basin widths. This excludes mechanisms based on spurious resonant phenomena taking place in the basin, due to particular combinations of geometric parameters.

Back to the 2 % steepness case, figure 7 shows, at different time instants ranging from arrival of the wavefront to occurrence of re-reflections, the free-surface RAO along the plate, compared with the predictions of linear theory and our parabolic model. The agreement with the linear prediction is rather good at the first two or

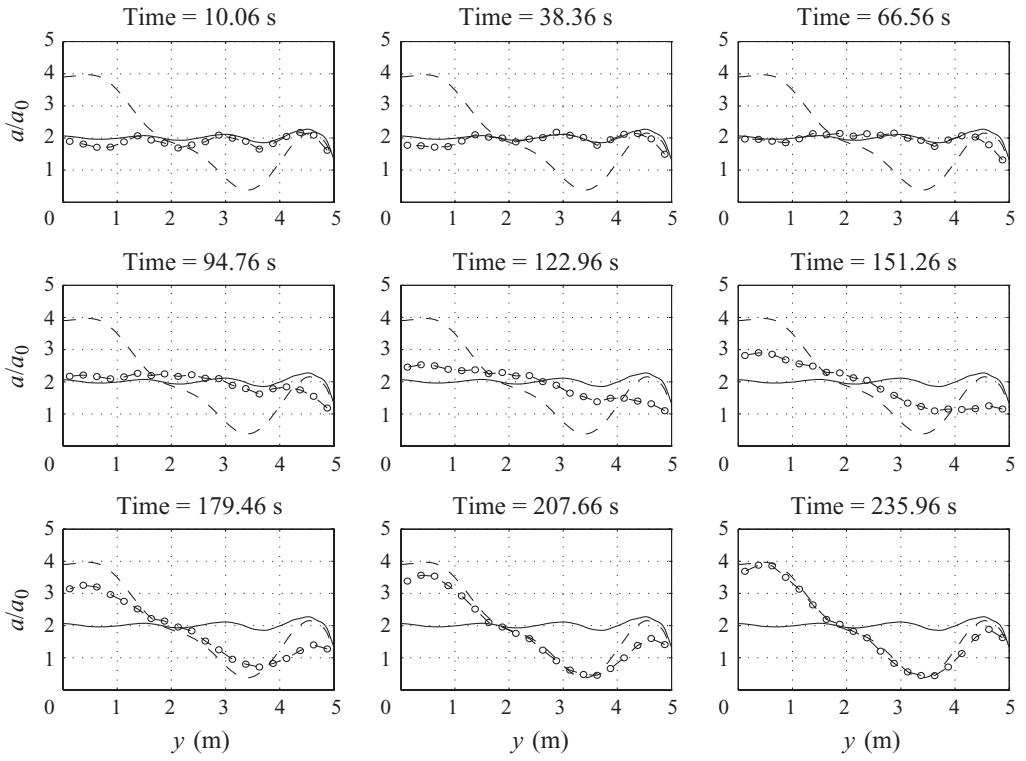

FIGURE 7. Wave period 1.01 s. Steepness $H/L = 2\,\%$. Time evolution of the free-surface elevation RAO along the plate from experiments (○), linear theory (solid line) and the parabolic model (dashed line).

three instants. By the last instant shown, the match between the experimental RAO and the parabolic model is quite remarkable (given the approximations inherent to the numerical model); it does look like the parabolic model provides the steady state solution that would be finally attained.

It is somewhat surprising that such nonlinear modifications of the wave profile along the plate are obtained at such a low wave steepness. In Molin *et al.* (2005*b*), nothing nonlinear could be seen at the 2 % steepness. Obviously, this is due to both the plate being much longer (relative to the wavelength) and the distance from the wavemaker to the plate being much larger.

To illustrate the effect of the interaction length, figure 8 shows the calculated RAOs along the plate, with the parabolic model, for interaction lengths ranging from 15 m to 200 m, that is from 9 to 125 wavelengths. The sensitivity of the RAOs to the interaction length is quite strong, and 100 m seems to be still too short for the full development of the nonlinear interactions between incoming and reflected wave fields. Note that these calculations have been done by keeping a constant width of the domain, equal to 30 m. They do not precisely reflect what would occur in open sea conditions because here the reflected wave energy remains confined to the tank walls.

Figures 9–12 are replicates of figure 7 for the other wave steepnesses of 2.5 %, 3 %, 3.5 % and 4 %. In the 4 % case, the plate had been moved 25 m closer to the wavemaker, due to the appearance of the Benjamin–Feir instability. In all figures

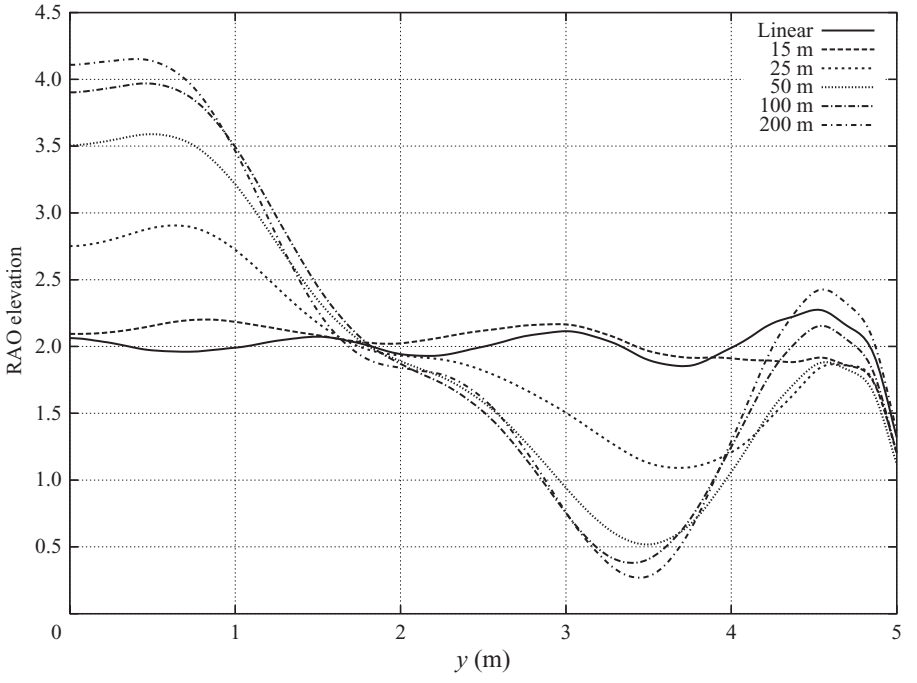

FIGURE 8. Wave period 1.01 s. Steepness $H/L = 2\,\%$. Free-surface RAOs obtained by the parabolic model for different interaction lengths.

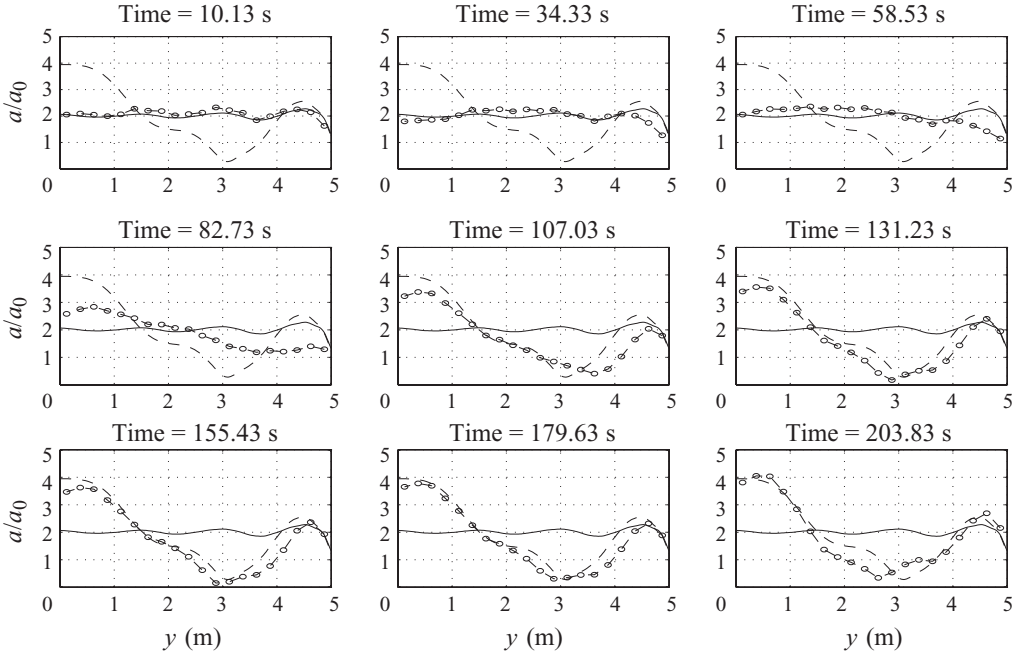

FIGURE 9. Wave period 1.01 s. Steepness $H/L = 2.5\,\%$. Time evolution of the free-surface elevation RAO along the plate from experiments (○), linear theory (solid line) and the parabolic model (dashed line).

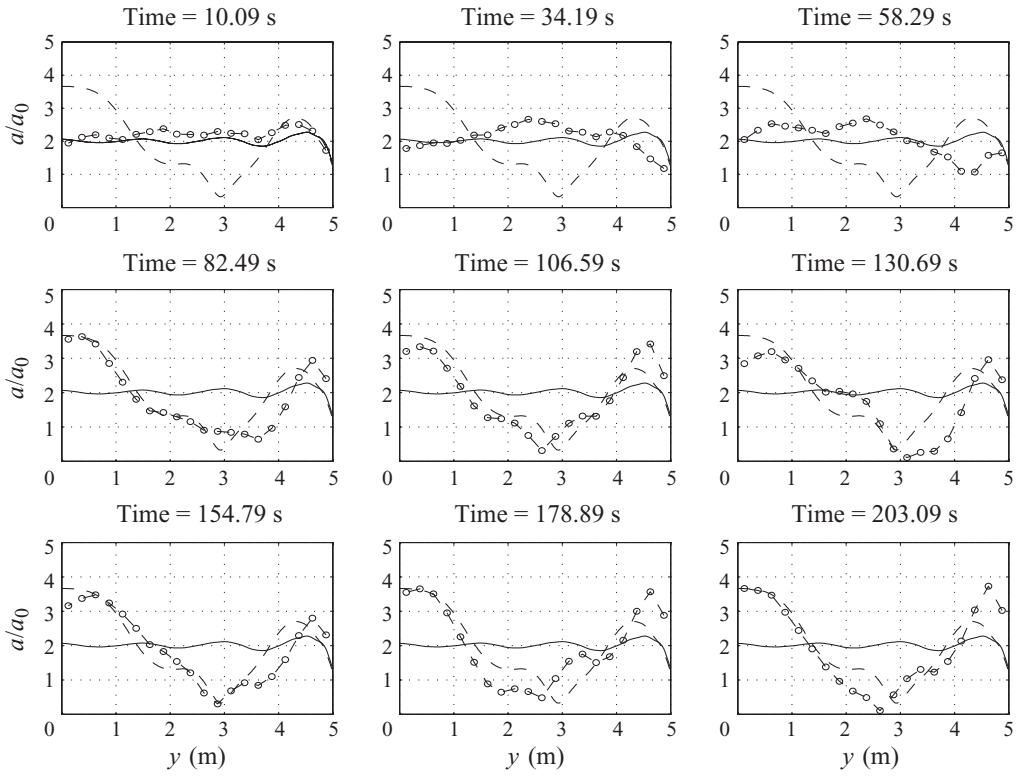

FIGURE 10. Wave period 1.01 s. Steepness $H/L = 3\,\%$. Time evolution of the free-surface elevation RAO along the plate from experiments (○), linear theory (solid line) and the parabolic model (dashed line).

except figure 12 (where convergence could not be reached) the profile given by the parabolic model is shown.

At the 2.5 % steepness, the experimental RAOs are rather close to the prediction of the parabolic model, from $t \sim 150$ s, with some oscillatory behaviour. The oscillatory behaviour is stronger at the 3 % steepness, with experimental peaks markedly larger than predicted by the parabolic model by the plate edge. At the 3.5 % steepness, the experimental RAOs are only qualitatively like the prediction of the parabolic model. At the first instant the measured RAOs are far above the linear prediction: this is due to the strong modulation of the wavefront and due to the measured wave amplitude during the calibration tests that is used to calculate the RAO (better visual agreement would be obtained by using the instantaneous amplitude as measured by the wave gauge away from the plate). Finally, at 4 %, even though the distance from the wavemaker to the plate has been decreased by 25 m, the experimental RAOs take on a chaotic appearance, with successive profiles quite different from the others. As discussed above, the iterative scheme implemented within the parabolic model failed to converge in that case, no matter how much relaxation was introduced, suggesting that no steady state can exist.

Finally, figure 13 gathers the free-surface RAOs along the plate, as obtained by the parabolic model, for the different wave steepnesses. It can be observed that the trough moves closer to the wall as the steepness increases. Correspondingly, the height of the

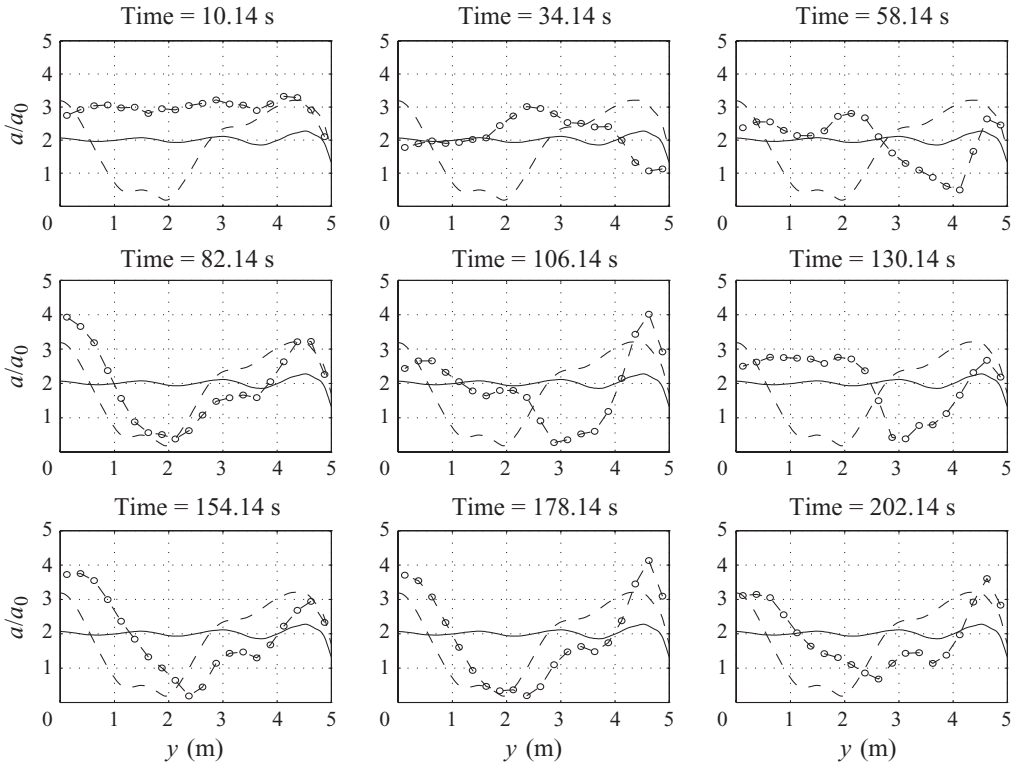

FIGURE 11. Wave period 1.01 s. Steepness $H/L = 3.5\,\%$. Time evolution of the free-surface elevation RAO along the plate, from experiments (○), linear theory (solid line) and the parabolic model (dashed line).

peak by the plate edge increases, while the height of the peak at the wall decreases. These features are well reproduced in the experiments.

4.2. *Regular wave tests at* 1.13 *s period*

In this section, we present some results from the tests performed in regular waves with a period of 1.13 s, meaning, according to linear theory, a wavelength of 2 m. The plate width over the wavelength ratio is the same as in the previous BGO-First tests (Molin *et al.* 2006) at the wave period of 0.88 s. The same numbers and positions (relative to the plate width) of wave gauges along the plates were used in both series of experiments.

4.2.1. *Comparison with the BGO-First model test results*

First, we show some comparative results of the two model tests. As observed above, the plate width over wavelength ratio is the same in both experiments (equal to 2.5), but the other geometric parameters are different: relative to the wavelength, the distance from wavemaker to plate is about 3 times larger in CEHIPAR, while the basin width is almost identical (12.5 % larger).

In figures 14, 15 and 16, we compare the time histories of the free-surface RAOs at every other gauge along the plates for the 2 %, 3 % and 4 % steepnesses, respectively. The time on the horizontal scale has been made non-dimensional by dividing it by the wave period. In the BGO-First experiments, re-reflections occur very quickly, after

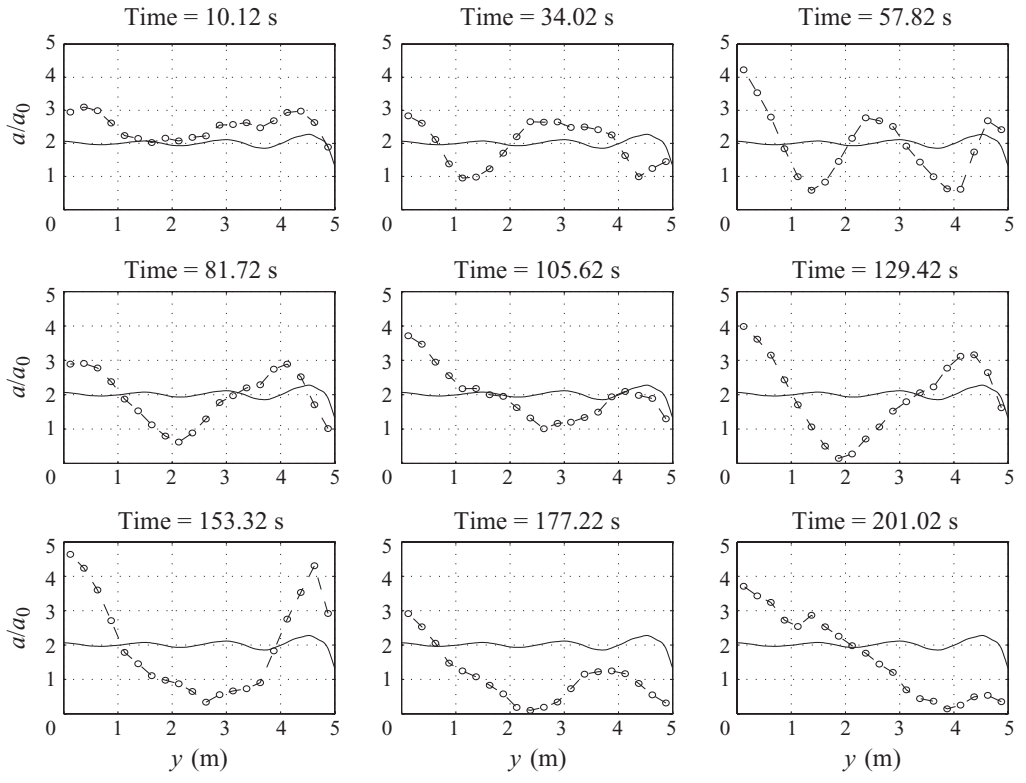

FIGURE 12. Wave period 1.01 s. Steepness $H/L = 4\,\%$. Time evolution of the free-surface elevation RAO along the plate from experiments (○) and linear theory (solid line). Plate moved at 75 m from the wavemaker.

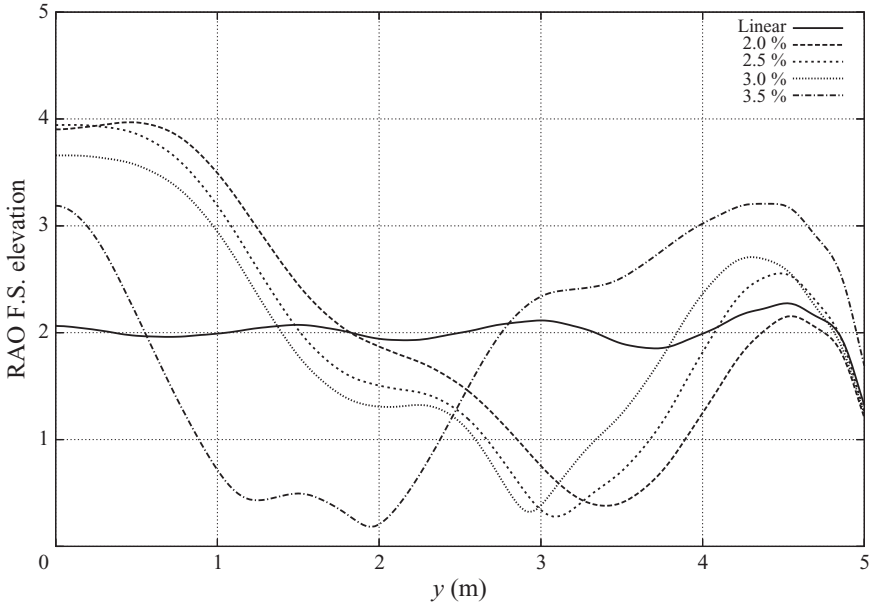

FIGURE 13. Wave period 1.01 s. Free-surface RAOs along the plate obtained by the parabolic model at interaction lengths of 100 m.

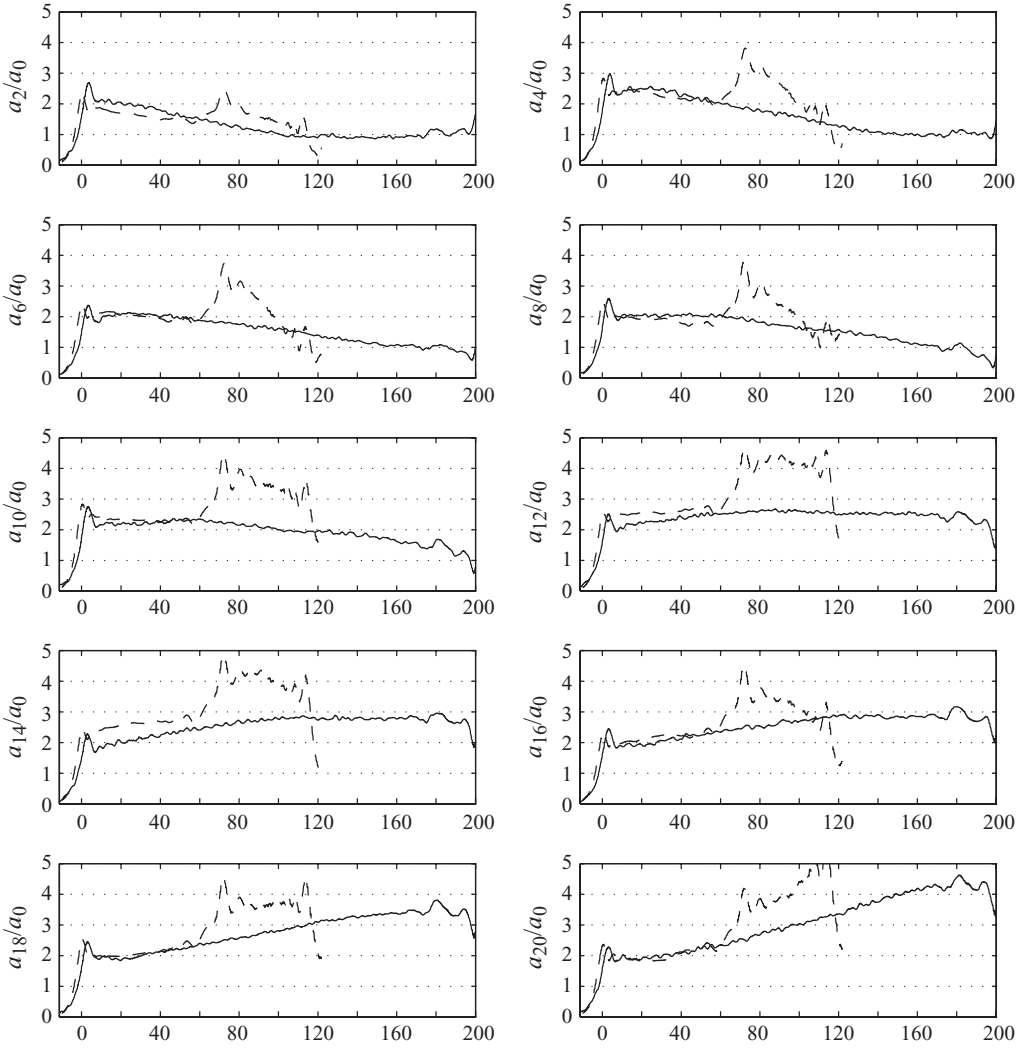

FIGURE 14. Wave period 1.13 s. Steepness $H/L = 2\,\%$. Time evolutions of the measured free-surface elevations RAOs at every other gauge from arrival of the wavefront. The solid line denotes CEHIPAR experiments and the dashed line denotes BGO-First experiments. (Horizontal scale is non-dimensional time t/T, T being the wave period.)

about 60 wave periods. In the CEHIPAR experiments, they occur after about 180 cycles.

At 2 % steepness (figure 14), the RAO time histories are nearly identical until the BGO-First ones get affected by re-reflections. The slight differences appearing at gauges 12 or 14 are presumably due to gauge calibration problems. As for gauge 2, the discrepancies may also be attributed to the different thicknesses of the two plates (1 cm at CEHIPAR, 5 cm at BGO-First). Other causes of discrepancies are that the wave steepnesses are not rigourously the same, and that the shapes of the wave fronts are different: because the waves travel a much longer distance in CEHIPAR before reaching the plate, more dispersive and nonlinear effects develop. This is probably the main reason for the comparatively larger differences that can be seen in figure 15,

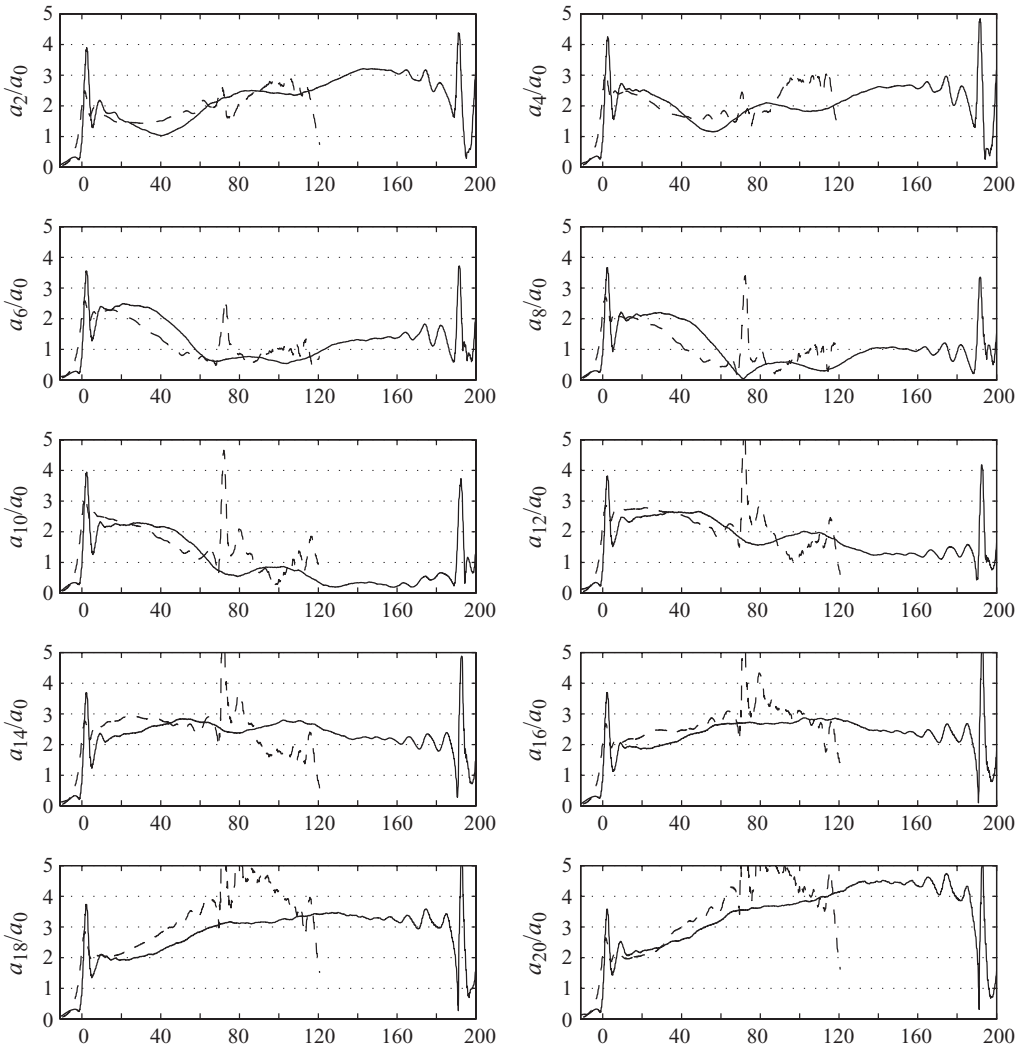

FIGURE 15. Wave period 1.13 s. Steepness $H/L = 3\,\%$. Time evolutions of the measured free-surface elevations RAOs at every other gauge from arrival of the wavefront. The solid line denotes CEHIPAR experiments and the dashed line denotes BGO-First experiments. (Horizontal scale is non-dimensional time t/T, T being the wave period.)

at the 3 % wave steepness, and, even more pronounced, in figure 16 at 4 % steepness. This last case was run twice, both at CEHIPAR and BGO-First; it can be seen from the figure that the repeatability is poor, actually poorer in BGO-First than at CEHIPAR. Most presumably, as argued about figures 3 and 4, this is due to the basins not being perfectly quiet at the start of the tests. The sensitivity of the RAO histories to the initial conditions seems to increase as the wave steepness becomes larger.

4.2.2. *Comparisons with the Boussinesq model*

The experimental wavetank at CEHIPAR was exactly reproduced in the computations, except that the part on the lee side of the plate was shortened, with the numerical damping zone starting 3 m from the plate and extending over

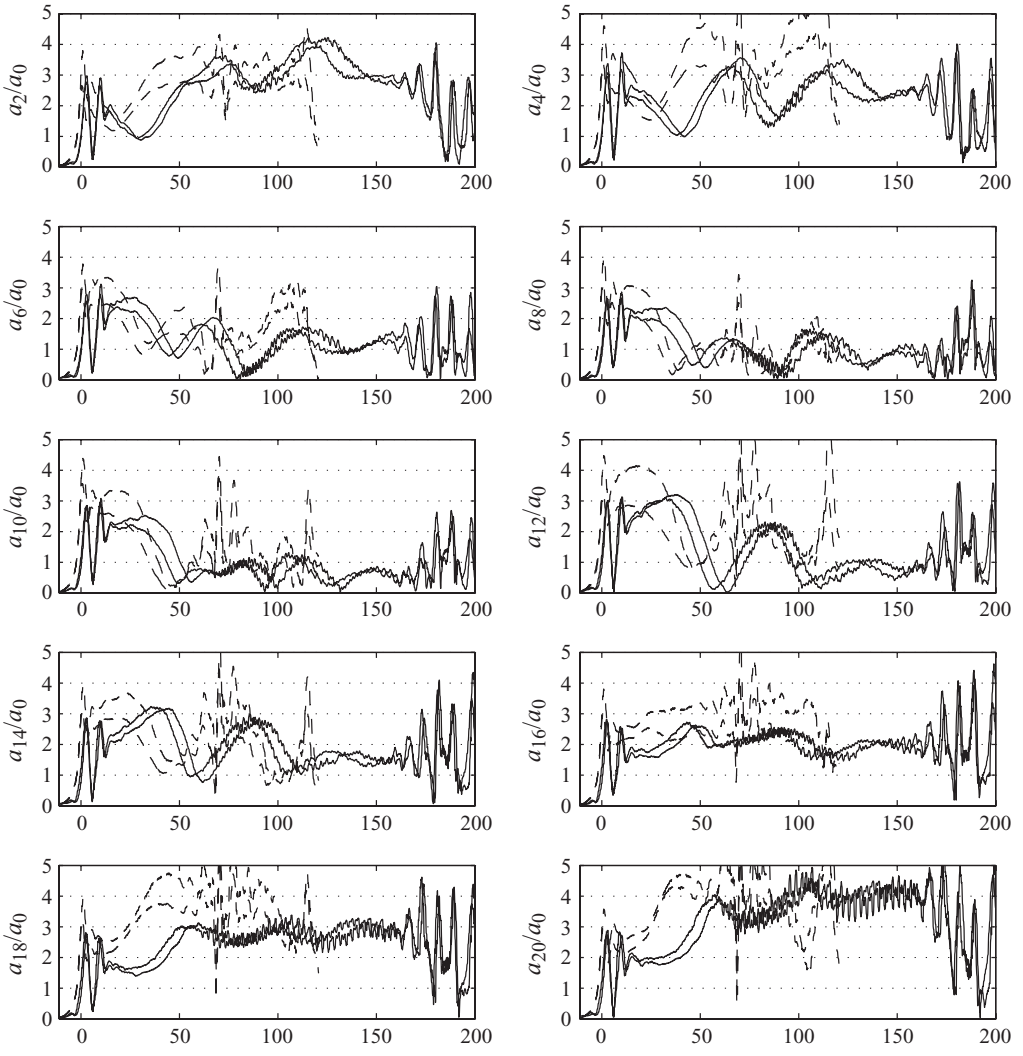

FIGURE 16. Wave period 1.13 s. Steepness $H/L = 4\,\%$. Time evolutions of the measured free-surface elevations RAOs at every other gauge from arrival of the wavefront. The solid line denotes CEHIPAR experiments and the dashed line denotes BGO-First experiments. (Horizontal scale is non-dimensional time t/T, T being the wave period.)

5 wavelengths. This means that the numerical domain had 56.5 wavelengths in the longitudinal direction and 15 wavelengths in the transverse direction. Twenty calculation points were taken per wavelength, that is 339 000 discretization points altogether, meaning 778 000 unknowns. It can be remarked here that twenty points per wavelength is too coarse to capture all nonlinear effects, for instance the second-order free waves at the double frequency 2ω are not properly reproduced (see Molin *et al.* 2005*a*). Refining the discretization would be computationally prohibitive, given the size of the domain. Fortunately, in deep water, these second-order free waves do not participate in the tertiary interaction effect that is the key to the phenomenon under study. The water depth was reduced so that kh takes the value of 5. The time step was taken equal to one-twentieth of the wave period.

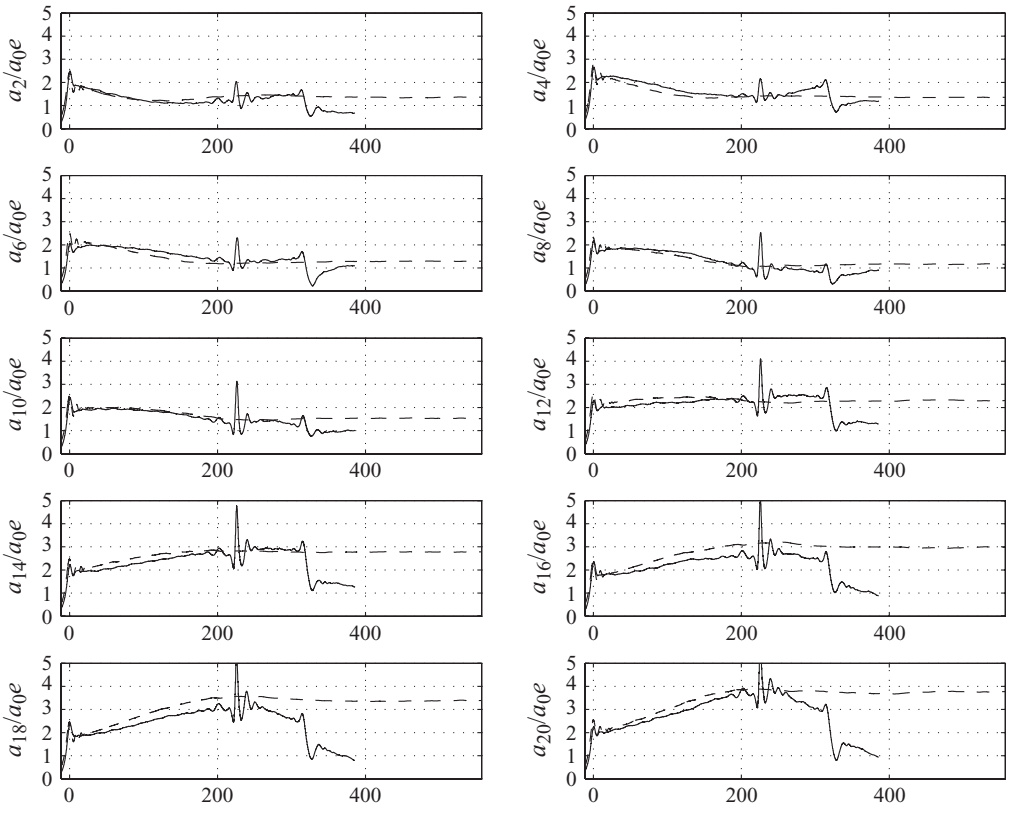

FIGURE 17. Wave period 1.13 s. Steepness $H/L = 2\,\%$. Time evolutions of the free-surface elevations RAOs at every other gauge from measurements (solid line) and the Boussinesq model (dashed line).

In the numerical wavetank, the incoming waves are gradually input over the first wavelength, from Fenton's streamfunction model (Fenton 1988). This generation zone is followed by a relaxation zone, 2 wavelengths long, where reflected waves by the plate are selectively damped out, unlike in the physical tank where they get re-reflected by the wavemaker. This permits us to continue the numerical simulation indefinitely and to check whether a steady state can be reached. The drawback is that these computations are quite demanding on computer resources: just to propagate the incoming waves from the wavemaker to the plate (a bit less than 2 min at CEHIPAR) takes 17 h on a 2.66 GHz double CPU workstation.

In the numerical model, the plate is thickened to the same value as the discretization step, that is 10 cm. The potential flow being singular at the two square corners, to avoid explicit calculations there, the plate walls are located half-way between grid points. Still the corner areas are prone to numerical instabilities and this is remedied by applying local filtering, which has the slight drawback of dissipating some energy. (Physically the flow locally separates at the square edges and this is a source of energy dissipation as well.)

Figure 17 shows the time evolution of the free-surface RAOs at every other gauge along the plate, as derived from measurements and as derived from the Boussinesq model, in the 2 % steepness case. The experimental and numerical time series were processed in the same way, i.e. Fourier analysis over sliding time window, three wave

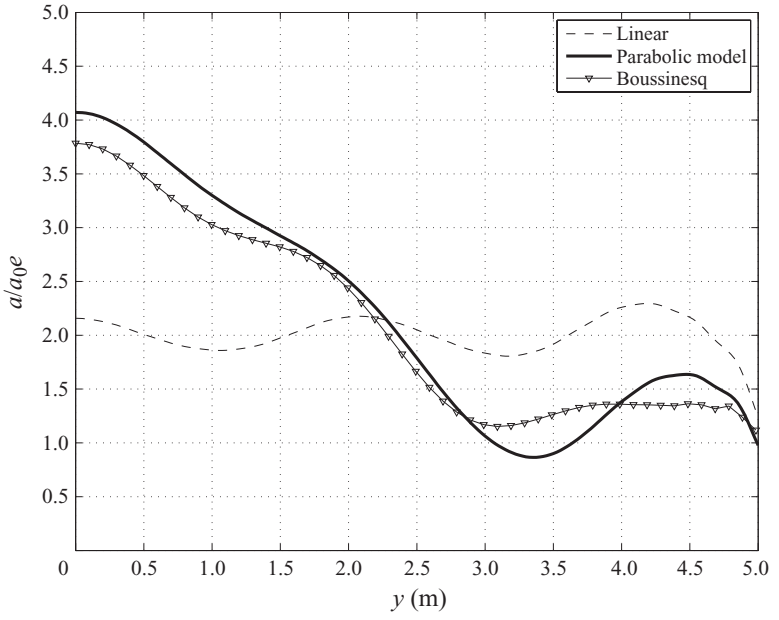

FIGURE 18. Wave period 1.13 s. Steepness $H/L = 2\,\%$. Free-surface RAOs along the plate from linear theory and the parabolic and Boussinesq models.

periods long. The numerical simulation has been pursued over more than 500 s after arrival of the wavefront. It can be seen that the two sets of curves are in fair agreement until the arrival of re-reflections in the experiments. Because of the selective damping zone, the numerical traces are not affected by this problem. Visually, it does look like the numerical RAOs stabilize in time and that a steady state is reached.

Figure 18 shows the free-surface RAO along the plate, obtained at the end of the Boussinesq simulation, compared with the parabolic model and with linear theory. The Boussinesq model, as compared to the parabolic one, underpredicts the height of the peak by the plate edge. This underestimation is presumably due to the numerical filtering that is applied by the plate edge. There are also discrepancies on the position and depth of the trough that appears at about 3 m from the wall. The remaining parts of the curves, from the wall to the trough are in fair agreement.

Figures 19 and 20 are replicates of figures 17 and 18 in the 2.5 % steepness case, while figures 21 and 22 show the 3 % steepness case. As the steepness increases, the discrepancies between the experimental and numerical time evolutions become larger. The reasons for these differences are, first, the experimental wave steepness, as derived from the calibration tests, which is known within some uncertainty margin, is estimated to be $\pm 5\,\%$. Second, as the wave steepness increases, the numerical wavefront, as it reaches the plate, increasingly differs from the experimental one, probably because the spatial and temporal discretizations are too coarse to capture all nonlinear effects that affect its evolution as it travels from the wavemaker to the plate. Finally, the sensitivity of the time evolution to the initial conditions gets larger as the wave steepness increases. In both steepness cases, the Boussinesq model predicts a steady state, with the transients lasting longer in the higher steepness case. Quite noticeable is the almost perfect node predicted by the parabolic model at the 3 % steepness (figure 22): it is somewhat unexpected that there can be, on the weather side of the plate, a location where the free-surface motion is nearly nil.

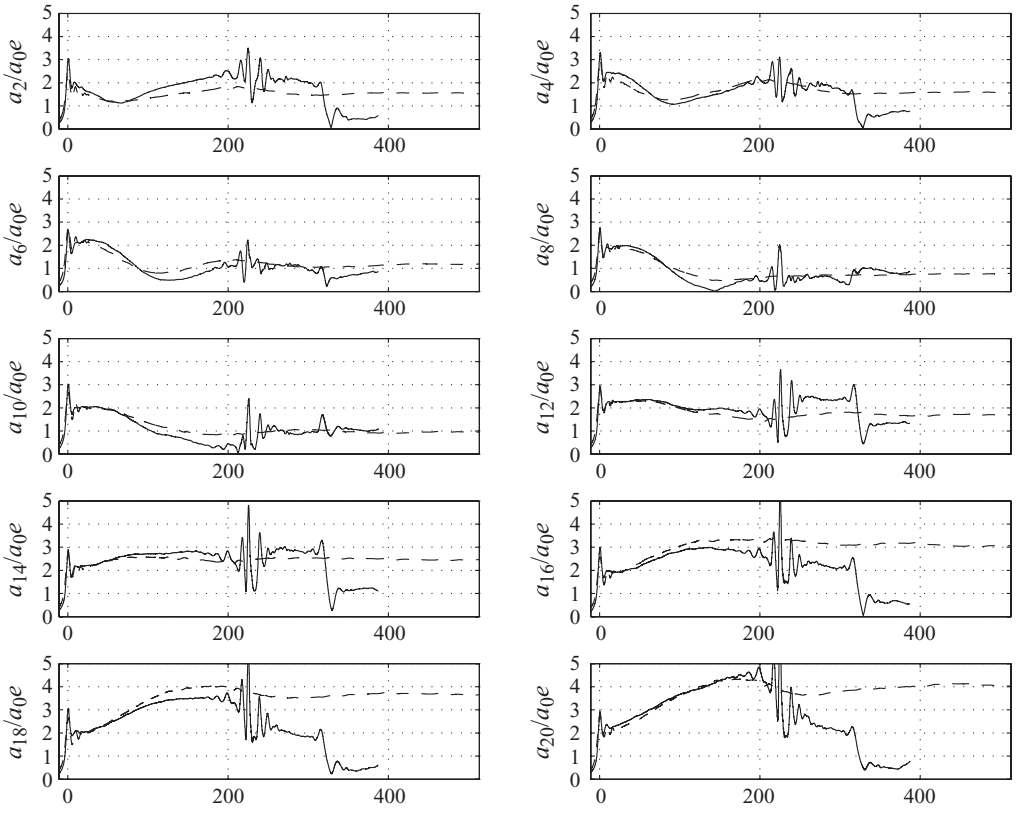

FIGURE 19. Wave period 1.13 s. Steepness $H/L = 2.5\,\%$. Time evolutions of the free-surface elevations RAOs at every other gauge from measurements (solid line) and the Boussinesq model (dashed line).

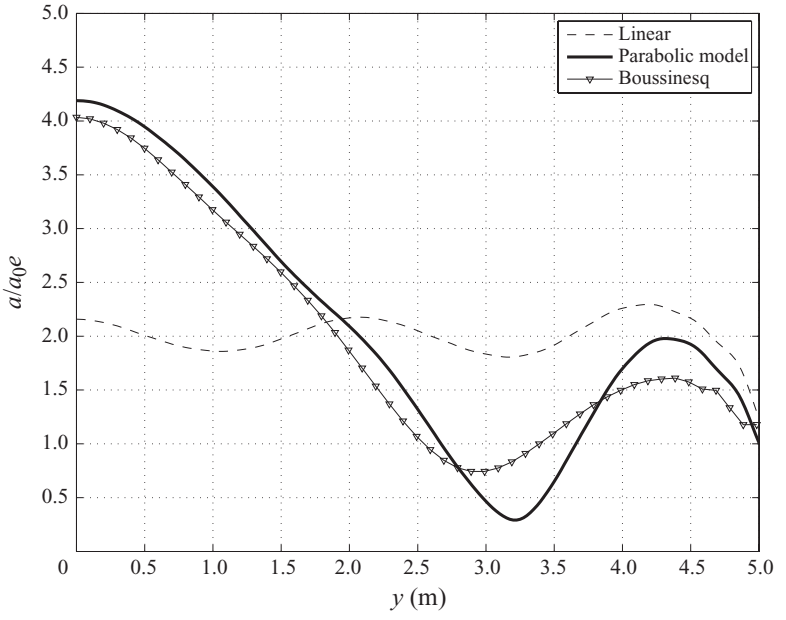

FIGURE 20. Wave period 1.13 s. Steepness $H/L = 2.5\,\%$. Free-surface RAOs along the plate from linear theory and the parabolic and Boussinesq models.

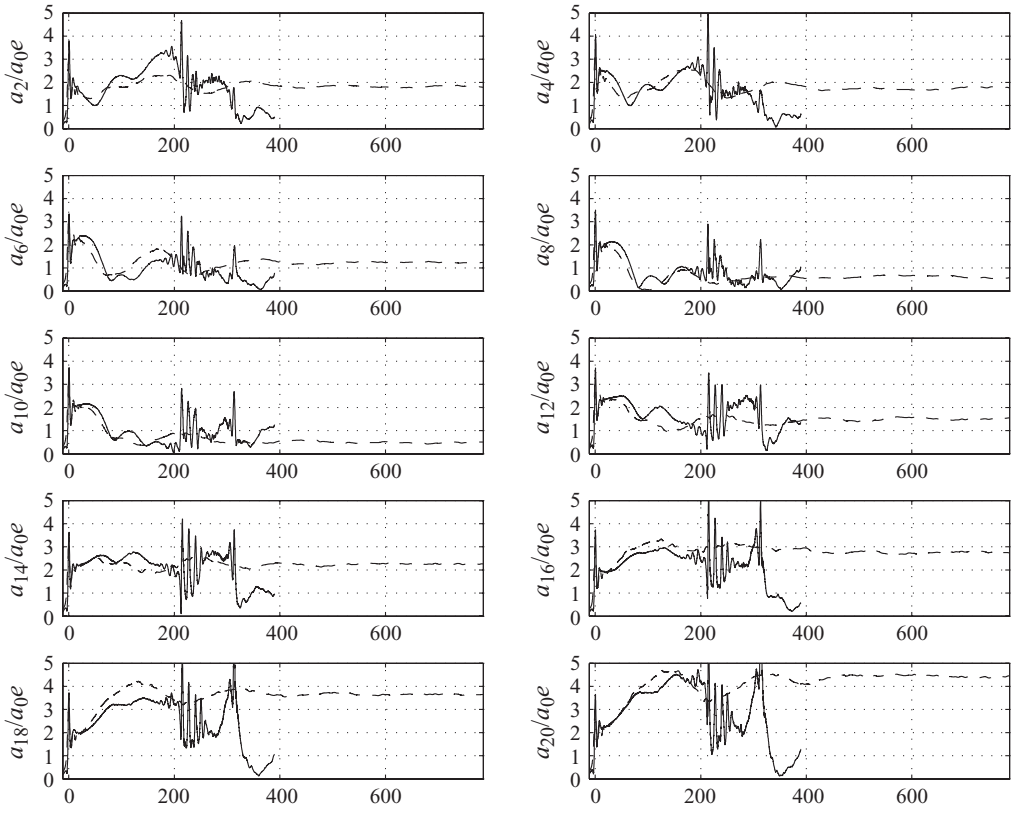

FIGURE 21. Wave period 1.13 s. Steepness $H/L = 3\,\%$. Time evolutions of the free-surface elevations RAOs at every other gauge from measurements (solid line) and the Boussinesq model (dashed line).

Finally, figure 23 shows a bird's eye view of the numerical basin in the 3 % steepness case.

Unfortunately, no numerical results can be shown at higher steepnesses because the numerical simulations break down after some time. This is attributed to the numerical waves becoming locally too steep. (Presumably, some wave breaking took place in the physical tank.) So the question whether steady states are attained at high wave steepnesses (where the iterative scheme implemented in the parabolic model fails to converge) is still open.

5. Final comments

The model test results and the comparisons made with the two numerical models confirm the original analysis given by Molin *et al.* (2005*b*): the time evolutions of the free-surface profiles along the plate are due to third-order interactions between the incident and reflected wave systems. The reflected waves slow down the incoming waves, with the same effect as a shoal; but it is a shoal that evolves in time as the reflected wave system progresses in the tank and as the incoming wave system undergoes modifications.

In Molin *et al.* (2005*b*), the plate was much shorter (1.2 m for wavelengths in the range 1.2–3 m); at low wave steepnesses ($H/L \sim 2\,\%$–$3\,\%$) hardly any nonlinear

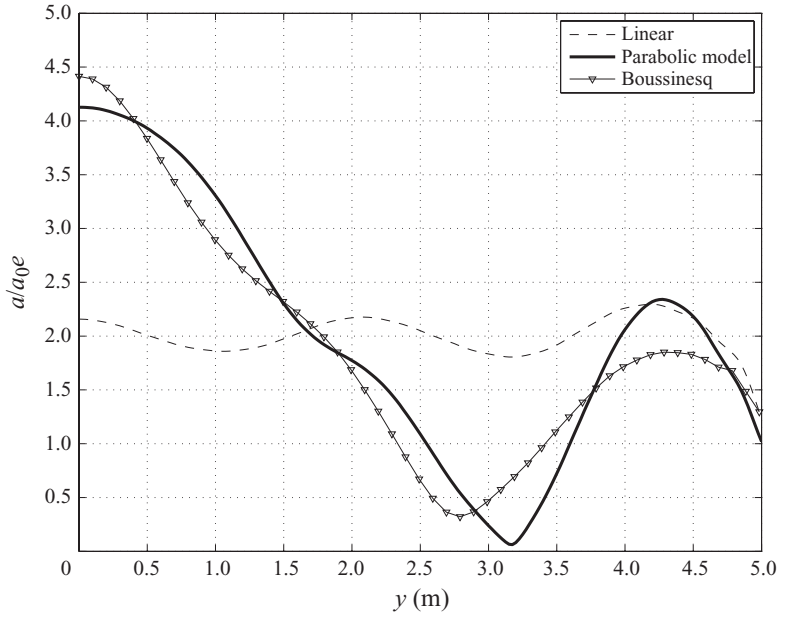

FIGURE 22. Wave period 1.13 s. Steepness $H/L = 3\,\%$. Free-surface RAOs along the plate from linear theory and the parabolic and Boussinesq models.

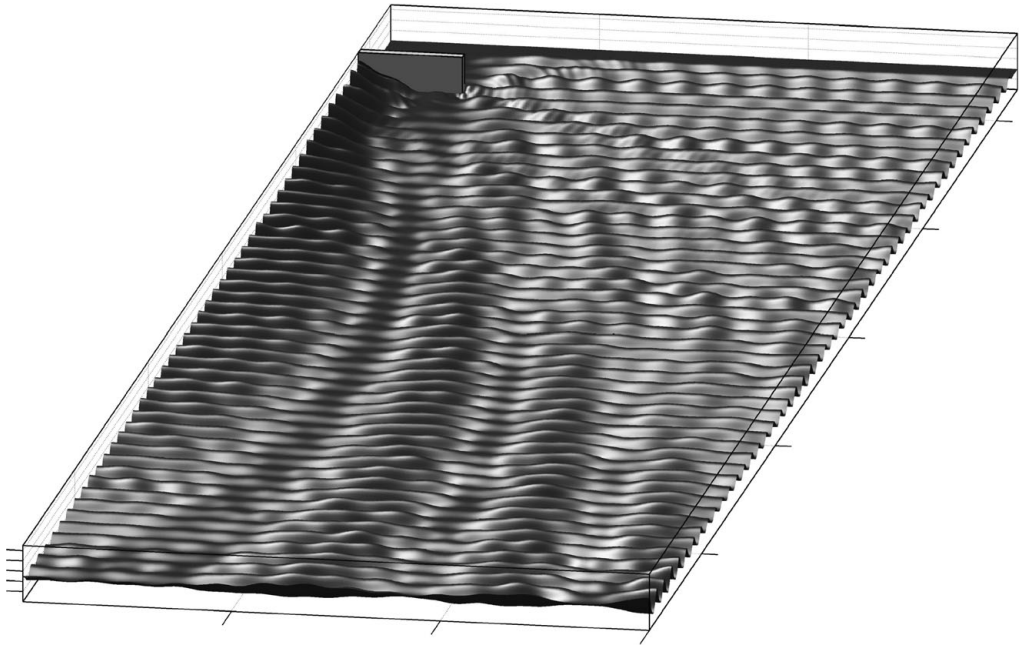

FIGURE 23. Wave period 1.13 s. Steepness $H/L = 3\,\%$. Three-dimensional view.

effect could be seen, transients were relatively short and the size of the interaction area, as predicted by the parabolic model, was a few wavelengths. In this new series of experiments, with a 5 m plate and wavelengths from 1.6 m to 2 m, conspicuous nonlinear evolution is observed at all wave steepnesses from $H/L = 2\,\%$, transients

seem to last for ever with no evidence of a steady state being attainable and the interaction area extends over more than 50 wavelengths: the CEHIPAR tank is still too small. The implications of these findings for model testing of long partially reflective structures, such as are being studied in coastal and port engineering (breakwaters, etc.), are tremendous. The numerical runs with the Boussinesq model suggest that the use of an actively controlled, absorbing wavemaker is strongly encouraged, but still this does not guarantee that the area from the wavemaker to the considered structure is of sufficient size to fully capture the nonlinear interaction between the incoming and reflected wave systems.

The Boussinesq model of Jamois (2005) turned out to perform remarkably well at the low wave steepnesses. Still, it can be improved in many ways. For instance less dissipative schemes can be derived for the treatment of exterior corners. We are also working on implementing local energy absorption mimicking the effect of wave breaking, that would allow to run the high wave steepness cases, and on simulating irregular wave systems. We are planning to report on these issues soon.

The work described in this publication was supported by the European Community's Sixth Framework Programme through the grant to the budget of the Integrated Infrastructure Initiative HYDRALAB III, contract 022441 (RII3). This document reflects only the authors' views and not those of the European Community. This work may rely on data from sources external to the HYDRALAB III project Consortium. Members of the Consortium do not accept liability for loss or damage suffered by any third party as a result of errors or inaccuracies in such data. The information in this document is provided "as is" and no guarantee or warranty is given that the information is fit for any particular purpose. The user thereof uses the information at its sole risk and neither the European Community nor any member of the HYDRALAB III Consortium is liable for any use that may be made of the information. The BGO-First model tests were carried out within the GIS-HYDRO organization, with financial support from Conseil Général du Var.

REFERENCES

Bingham, H. B., Madsen, P. A. & Fuhrman, D. R. 2009 Velocity potential formulations of highly accurate Boussinesq-type models. *Coast. Engng* **56**, 467–478.

Dingemans, M. W. 1997 *Water Wave Propagation over Uneven Bottoms. Part 1. Linear Wave Propagation.* World Scientific.

Fenton, J. D. 1988 The numerical solution of steady water wave problems. *Comput. Geosci.* **14**, 357–368.

Fuhrman, D. R. & Bingham, H. B. 2004 Numerical solutions of fully nonlinear and highly dispersive Boussinesq equations in two horizontal dimensions. *Intl J. Numer. Meth. Fluids* **44**, 231–255.

Jamois, E. 2005 Interaction houle-structure en zone côtière. PhD thesis, Aix-Marseille II University, CEDERS (in French).

Jamois, E., Fuhrman, D. R., Bingham, H. B. & Molin, B. 2006 A numerical study of nonlinear wave run-up on a vertical plate. *Coast. Engng* **53**, 929–945.

Longuet-Higgins, M. S. & Phillips, O. M. 1962 Phase velocity effects in tertiary wave interactions. *J. Fluid Mech.* **12**, 333–336.

Molin, B., Jamois, E., Lee, C.-M. & Newman, J. N. 2005*a* Nonlinear wave interaction with a square cylinder. In *Proceedings of the 20th International Workshop on Water Waves and Floating Bodies*, Longyearbyen (ed. J. Grue) (www.iwwwfb.org).

Molin, B., Kimmoun, O., Remy, F. & Jamois, E. 2006 Nonlinear wave interaction with a long vertical breakwater. In *Proceedings of the Seventh International Conference on Hydrodynamics, ICHD 2006* (ed. P. Cassella & P. Cioffi), vol. 1, pp. 11–18.

Molin, B., Remy, F., Kimmoun, O. & Jamois, E. 2005*b* The role of tertiary wave interactions in wave-body problems. *J. Fluid Mech.* **528**, 323–354.

Radder, A. C. 1979 On the parabolic equation method for water-wave propagation. *J. Fluid Mech.* **95**, 159–176.

Spentza, E. & Swan, C. 2009 Wave–vessel interactions in beam seas. In *Proceedings of the 28th ASME International Conference on Ocean, Offshore and Arctic Engineering* (ed. ASME), compact disc, OMAE2009-79605.

Zakharov, V. E. 1968 Stability of periodic waves of finite amplitude on the surface of a deep fluid. *J. Appl. Mech. Tech. Phys.* **9**, 190–194.